Engineering Computations

Computational study of a dorsolumbar complete burst fracture and its fixation methods

Rita Moura and Daniel Fidalgo
Faculdade de Engenharia, Universidade do Porto, Porto, Portugal and INEGI, Porto, Portugal
Dulce Oliveira
INEGI, Porto, Portugal
Ana Rita Reis
Faculdade de Engenharia, Universidade do Porto, Porto, Portugal
Bruno Areias
INEGI, Porto, Portugal
Luísa Sousa
Faculdade de Engenharia, Universidade do Porto, Porto, Portugal
João M. Gonçalves
Hospital da Luz, Vila Nova de Gaia, Portugal
Henrique Sousa
Centro Hospitalar de Vila Nova de Gaia Espinho EPE, Vila Nova de Gaia, Portugal, and
R.N. Natal Jorge and Marco Parente
Faculdade de Engenharia, Universidade do Porto, Porto, Portugal

Received 20 December 2023
Revised 30 April 2024
Accepted 7 June 2024

Abstract

Purpose – During a fall, a significant part of the major forces is absorbed by the dorsolumbar column area. When the applied stresses exceed the yield strength of the bone tissue, fractures can occur in the vertebrae. Vertebral fractures constitute one of the leading causes of trauma-related hospitalizations, accounting for 15% of all admissions. Posterior pedicle screw fixation has become a common method for treating burst fractures. However, physicians remain divided on the number of fixed segments that are needed to improve clinical outcomes. The present work aims to understand the biomechanical impact of different fixation methods, improving surgical treatments.

Design/methodology/approach – A finite element model of the dorsolumbar spine (T11–L3) section, including cartilages, discs and ligaments, was created. The dorsolumbar stability was tested by comparing two different surgical orthopedic treatments for a fractured first lumbar vertebra on the L1 vertebra: the posterior

The authors gratefully acknowledge the support from the Portuguese Foundation of Science under the Grants 10.54499/2020.05400.BD and 10.54499/2021.05876.BD, the Junior Researcher Contract 10.54499/2020.01522.CEECIND/CP1612/CT0001, the funding of Project UIDB/50022/2020 and the European Union's Horizon 2020 research and innovation program, under grant agreement No 953169 within the scope of the InterLynk project.

Engineering Computations
Emerald Publishing Limited
0264-4401
DOI 10.1108/EC-12-2023-0943

short segment fixation with intermediate screws (PSS) and the posterior long segment fixation (PL). Distinct loads were applied to represent daily activities.
Findings – Results show that both procedures provide acceptable segment fixation, with the PL offering less freedom of movement, making it more stable than the PSS. The PL approach can be the best choice for an unstable fracture as it leads to a stiffer spine segment.
Originality/value – This study introduces a novel computational model designed for the biomechanical analysis of dorsolumbar injuries, aiming to identify the optimal treatment approaches within both clinical and surgical contexts.

Keywords Biomechanics, Vertebral column, Posterior long segment fixation,
Posterior short segment fixation with intermediate screws, Finite element model, Numerical simulation
Paper type Research paper

1. Introduction

The spine provides structural support and protects neurons that transmit information to and from the brain. It is divided into five regions: cervical (C1–C7), thoracic (T1–T12), lumbar (L1–L5), sacral (S1–S5, fused together) and coccygeal (Frost *et al.*, 2019). The lumbar spine is continually in motion and bears the full weight of the upper body, making it particularly susceptible to injuries (Mahadevan, 2018). Low back pain can be characterized as an ache in the lumbar portion of the spine. It becomes more common with advancing age, and its prevalence rate can range from 4 to 69%. Furthermore, low back pain is the leading cause of musculoskeletal disability (Vos *et al.*, 2017).

A high impact fall can lead to spine fractures, which accounted for 15% of all trauma hospitalizations in 2019 (Hershkovitz *et al.*, 2021). According to the AO thoracolumbar fracture classification (the most used thoracolumbar spinal fracture classification system), injuries can be categorized into three groups (A – compression injuries, B – distraction injuries and C – translation injuries). When multiple levels are injured, each injury is classified separately and should be reported in order of declining severity. Type A injuries involve the vertebral body and have five levels of severity (A0–A4). A complete burst fracture (Type A4) is a fracture that involves both endplates along with the posterior vertebral wall (Vu and Gendelberg, 2020). For the majority of stable burst Type A fractures, successful treatment often involves pain medication, rest and bracing (Jay and Ahn, 2013). If, within 4–6 weeks, this conservative approach fails to restore bone union and spinal stability, surgery is recommended (Minamide *et al.*, 2018). Therefore, conservative treatment is generally considered for stable fractures, while surgical intervention is recommended for unstable fractures (Soultanis *et al.*, 2021).

The two most widely used surgical methods for the treatment of an unstable A4 fracture are posterior short segment fixation with intermediate screws (PSS) and posterior long segment fixation (PL). The PSS procedure initiates with the insertion of pedicle screws in the L2 and T12 vertebrae, intermediate screw placement in the fractured L1 vertebra, followed by rod contouring, rod insertion and subsequent decompression and distraction. Some studies compare this procedure with a similar one that does not involve intermediate pedicle screws. Tian *et al.* (2011) concluded that the PSS procedure restores fractured vertebral height efficiently, allowing earlier ambulation, and is also associated with a decrease in the segmental kyphotic angle. The intermediate screws provide more biomechanical stability to the construct than the traditional posterior short segment fixation (Tian *et al.*, 2011). Conversely, in the PL approach, no screws are placed in the injured vertebra. Instead, screws are inserted in the two vertebrae above and below the fractured L1, specifically in the T11, T12, L2 and L3 vertebrae. In both cases, the instrumentation is removed 9–18 months after the surgery, when the vertebra has completely healed (Liang *et al.*, 2020).

Computational simulations can be a powerful tool to study spine biomechanics. Understanding the biomechanical characteristics of the human spine is critical when

choosing the treatment for spine pathology. Finite element (FE) numerical simulations allow estimation of displacements, strain and stress distributions with low costs and no risks to the biological tissue.

Several works have used FE numerical simulations to investigate spine biomechanics. Zhang and Zhu (2019) developed a three-dimensional nonlinear FE model of the lumbosacral vertebrae to explore the path of the follower load, a compressive load of physiologic magnitude acting on the whole spine, which remains unclear. Additionally, addressing the influence of material and morphological parameters on the mechanical response of the lumbar spine, Zander *et al.* (2017) established an FE model to ascertain the sensitivities of spinal forces and motions to material parameters of intervertebral discs, vertebrae and ligaments as well as to lumbar morphology. Sohn *et al.* (2018) developed a three-dimensional nonlinear FE model of the lumbosacral spine with the aim of characterizing the biomechanical properties of a modified iliac screw fixation method compared to the classic iliac screw fixation.

Furthermore, FE models have also been developed to investigate the impact of several clinical interventions on the biomechanics of the human spine in the short and long term. Fidalgo *et al.* (2020) developed a numerical model comprising the L5, sacrum and intervertebral disk to investigate the impact of minimally invasive transforaminal and anterior lumbar interbody fusion surgeries. Similarly, Areias *et al.* (2020) developed a model comprising the L4 and L5 vertebrae to study lateral and transforaminal lumbar interbody fusion. Svedmark *et al.* (2012) aimed to assess segmental movement in the lumbar spine with computed tomography in healthy subjects and to determine rotation accuracy on phantom vertebrae.

The main goal of the current study is to conduct a comparative analysis of the mobility of vertebrae facilitated by two different posterior fixation methods (PSS and PL). This work aims to offer valuable insights into the relative efficacy and implications of these two fixation techniques in the context of spine biomechanics, determining which approach is more suitable from a biomechanical perspective.

2. Materials and methods

A FE model of the dorsolumbar spine was created using computed tomography (CT) images and designated as the control model, considered healthy. Subsequently, a second model was appropriately modified based on the control model to simulate an unstable complete burst fracture on the L1 vertebra, resulting in the injured model. The injured model underwent posterior modifications to simulate two posterior fixation approaches: PSS and PL.

In this section, the distinct models are described and a detailed description of the boundary conditions, interactions and mechanical properties applied in each case is provided.

2.1 Control model

The anatomical structures of the vertebrae were reconstructed utilizing high-resolution CT-scan images with a slice thickness of 0.5 mm. These scans were obtained from a 30-year-old male without any recent spine-related issues, ensuring a baseline representation of healthy anatomy. The image processing was conducted using Mimics® software within a defined region of interest spanning from the T11 to L3 vertebrae. To enhance the clarity and accuracy of the reconstructed images, several processing steps were employed. Contrast adjustments were calibrated to optimize visibility, while Gaussian filters were applied to reduce noise and enhance image sharpness. Additionally, morphological filters were utilized to refine the contours and structures of the vertebrae, resulting in a more precise representation. The final output comprised segmented masks of the vertebrae, isolating them from surrounding

tissues and artifacts. This segmentation was crucial for subsequent analyses and measurements. Notably, the thresholding parameters used for segmentation adhered to the default settings of the Mimics® software, ensuring consistency and reproducibility in the process.

The resultant files were exported containing the 3D shell of each vertebra and imported to the Autodesk Meshmixer software for deleting intersections and achieving a smooth triangular surface. Finally, four-node tetrahedral elements (C3D4) were used to mesh each vertebra in Abaqus® software. The elements were differentiated in trabecular (inner elements) and cortical bone (outer elements), according to the histogram values of the CT images. Figure 1 presents the FE model of the dorsolumbar healthy column.

The geometry of the intervertebral discs was defined using the lower surface of T11 and the upper surface of T12. A plane was defined slightly below the lower surface of T11 and the disc geometry was obtained by extruding the elliptical sketch in direction to T12 and extending slightly above the superior endplate of T12. This procedure was repeated in all spaces between the vertebrae, namely T12–L1, L1–L2 and L2–L3 functional spine units (FSU), making a total of four intervertebral discs (as can be seen in Figure 1). Chen *et al.* (2001) defined the nucleus pulposus as 30–50% of the total disc volume. Similarly, in this study, the volume delimited by the inner surface of the annulus fibrosus corresponds to 40% of the total disk volume. The volume bounded by the inner and outer annulus fibrosus surfaces was then divided into eight layers, as shown in Figure 2, with an average sectional area of 76.41 mm^2, resembling the fibers of the disc.

As reported by Marchand and Ahmed (1990), there are many crosslinked fibers that would be almost impracticable to replicate. Nonetheless, the same authors detected up to eight peripheral layers, also simulated in this work. Their study mentioned that the average fiber

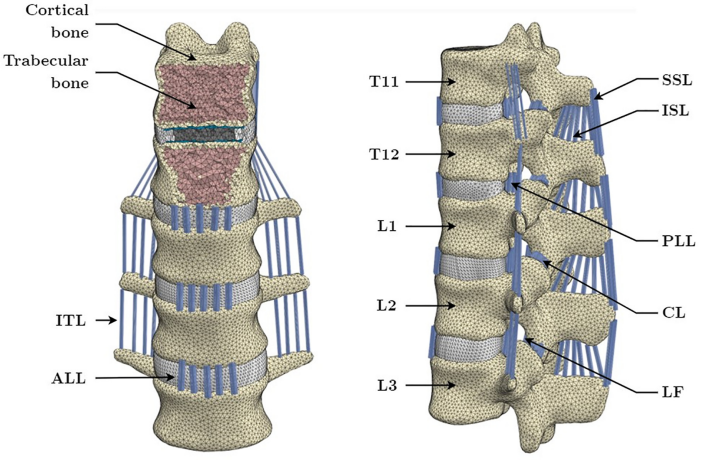

Note(s): Representation of the Anterior Longitudinal (ALL), Intertransverse (ITL), Supraspinous (SSL), Interspinous (ISL), Capsular (CL), Flavum (LF) and Posterior Longitudinal (PLL) ligaments.
(a) Anterior view with a section cut to demonstrate the trabecular (inner elements) and cortical bone (outer elements). (b) Lateral view

Source(s): Authors' own creation

Figure 1.
FE model of the dorsolumbar column, where it is identified the different vertebrae: the 11th and 12th thoracic (T11 and T12), the first, second and third lumbar (L1, L2 and L3)

bundle angle corresponded to 30° to the horizontal plane. These collagen fibers reinforce the viscous annulus by creating a crisscrossing network. To mimic this aspect, the orientation of the fibers alternates from layer to layer, oriented at an angle of ±30° with respect to the horizontal plane. In Figure 2, the fibers in grey elements represent the −30° oriented fibers and the white elements the 30° oriented fibers, as demonstrated. Between the disc and the vertebral endplate resides the cartilaginous endplate, which covers the nucleus and the inner fibers of the disc. Two cartilaginous plates were modeled in the superior and inferior disc surfaces, with a thickness between 0.5 and 1 mm (Moon *et al.*, 2013; Wade, 2018).

The seven major ligaments that hold the vertebrae together and stabilize the spine were also modeled: the anterior longitudinal ligament (ALL), capsular ligament (CL), interspinous ligament (ISL), intertransverse ligament (ITL), ligamentum flavum (LF), posterior longitudinal ligament (PLL) and supraspinous ligament (SSL), shown in Figure 1. These ligaments were modeled using two-node tension-only truss elements (Abaqus T3D2 element) in Abaqus® software. Each ligament was considered a group of separate lines, and posteriorly each line was meshed with a single finite element, according to Moramarco *et al.* (2010). Table 1 shows the ligaments cross-sectional area in mm^2 (Cheung *et al.*, 2003).

2.2 Unstable complete burst fracture model

Figure 3 demonstrates the FE model of the pathological model, corresponding to a dorsolumbar column with an unstable complete burst fracture of Type A4 on the L1 vertebra.

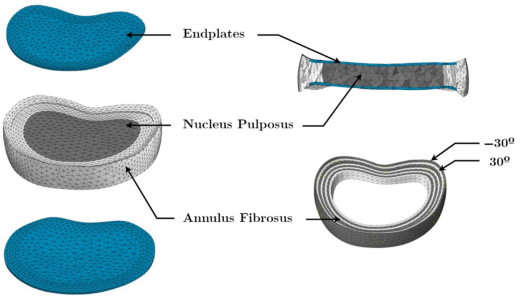

Source(s): Authors' own creation

Figure 2. Intervertebral discs composed by nucleus pulposus and annulus fibrosus and cartilaginous endplates

Component	Young modulus [MPa]	Poisson ratio [−]	Section area [mm^2]
Cortical bone	12,000	0.3	–
Trabecular bone	100	0.2	–
Cartilaginous endplates	24	0.4	–
Anterior longitudinal (ALL)	11.9	0.3	8.00
Capsular (CL)	7.7	0.3	5.00
Interspinous (ISL)	3.4	0.3	6.67
Intertransverse (ITL)	3.4	0.3	2.50
Flavum (LF)	2.4	0.3	13.33
Posterior longitudinal (PLL)	12.5	0.3	4.00
Supraspinous (SSL)	3.4	0.3	10.00
Screws and rods	110,000	0.3	–

Note(s): Geometrical properties of the ligaments
Source(s): Authors' own creation

Table 1. Mechanical properties of the bone, cartilaginous endplates, ligaments, fixation rods and screws

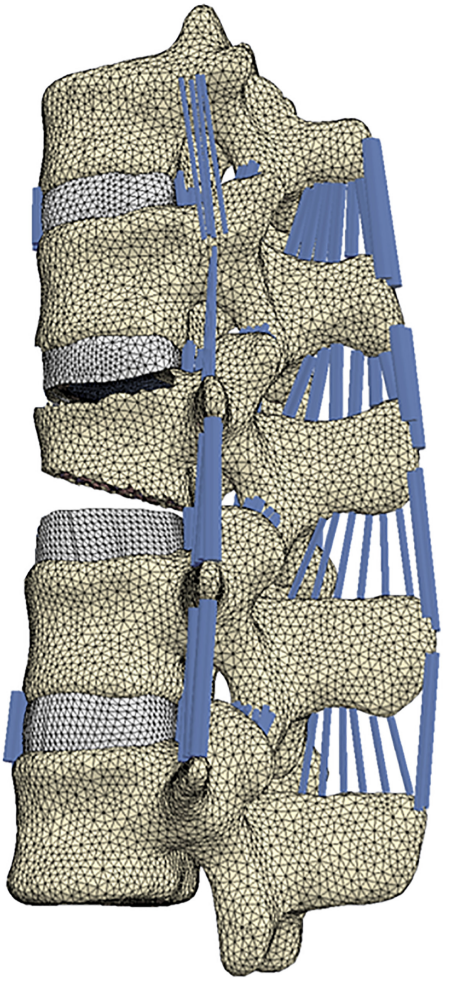

Source(s): Authors' own creation

Figure 3.
FE model of the dorsolumbar column representing the unstable complete burst fracture of type A4 on the L1 vertebra

Both superior and inferior pairs of vertebral and cartilaginous endplates of the L1 vertebra were removed from the initial model, following Wang *et al.* (2019) approach. Furthermore, the lower third of the L1 vertebral volume and the ALL ligaments of T12–L1 and L1–L2 were not considered to simulate an unstable complete burst fracture.

2.3 Fixation techniques

For the PSS fixation, the T11 and L3 vertebrae remained similar to the initial model, as screws were inserted into the remaining ones (T12, L1 and L2). Regarding the PL fixation, screws were placed in all vertebrae except for L1, which sustained the fracture.

The diameter of the screws was chosen based on the pedicle width, ensuring it is at least 0.5 mm smaller than the outer pedicle to ensure a safe transpedicular screw installation (Fujimoto *et al.*, 2012). Additionally, it is crucial to measure the distance from the outer pedicle to the anterior cortical area to determine the appropriate pedicle screw length, preventing

vascular or visceral complications (Bianco *et al.*, 2019; Vaccaro *et al.*, 1995). Dorsolumbar screws can range from 4.0 mm to 6.5 mm in diameter and 30 mm–45 mm in length (Lenke and Kim, 2005; Zhifeng *et al.*, 2018). Taking this into account, the selected screws have a diameter of 5.5 mm and a length of 45 mm. The FE mesh of a single screw is shown in Figure 4a.

Each screw, designed with the specified dimensions, was modeled in Solidworks to accurately replicate all its major geometrical characteristics. Subsequently, the screws were incorporated into the pathological model in accordance with the surgical procedure – six screws for the PSS and eight screws for the PL approach. Following this, each screw was positioned on its respective vertebra and meshed using Abaqus® software.

To correctly position the screws, a parallel plane to each superior endplate was created (Lehman *et al.*, 2003). This plane intersected with the inferior edge of the transverse process for thoracic vertebrae and the midpoint of the transverse process for lumbar vertebrae. To determine the positioning direction conclusively, considering the pedicle's anatomy, the screw's convergence angle was measured from the outer cortical plane to the sagittal middle section, ensuring it did not exceed (Fennell *et al.*, 2014). The final position of the screws is shown in Figure 4b, with the T12 vertebra, as an example for all the vertebrae that underwent screw placement.

Once the screws were inserted, each posterior surface was connected with a rod. These were meshed with B31 beam elements, featuring circular sections with a diameter of 5.5 mm. This type of element gives rigidity to the beam elements across all axes. The final models for the PSS and PL approaches are illustrated in Figure 5.

2.4 Boundary conditions and interactions

Boundary conditions were defined considering that all nodes of the inferior endplate of the L3 vertebra were fixed, which constrained it from moving in any direction.

Loads were applied at a reference point (P) located at the center of the superior T11 endplate (Figure 4c). The coupling function, available in Abaqus®, was utilized to distribute the load from the reference point to all superior endplate nodes of the T11 vertebra. At this reference point, a load of 5 Nm was applied for flexion, extension, lateral bending and axial rotation motions (Couvertier *et al.*, 2017), as demonstrated in Figure 6.

The interfaces of the intervertebral disc and the insertion points of the ligaments were attached to the vertebrae using a tie constraint to prevent relative motion between contact

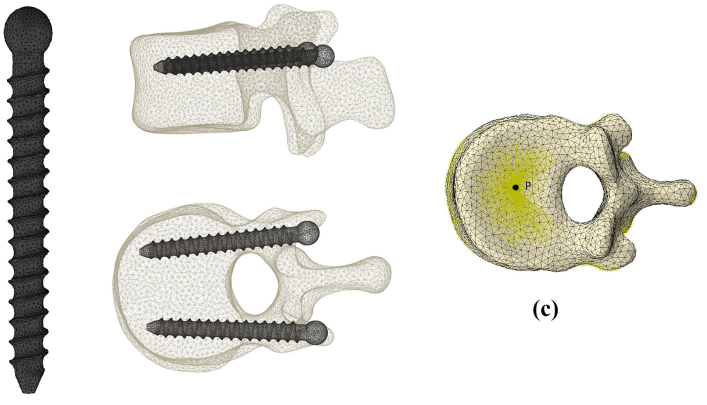

Source(s): Authors' own creation

Figure 4.
(a) FE single screw model with 5.5 mm of diameter and 45 mm length. (b) lateral and superior views of the screws' positioning in the T12 vertebra. (c) Reference Point, P, on the T11 superior endplate for the posterior load application

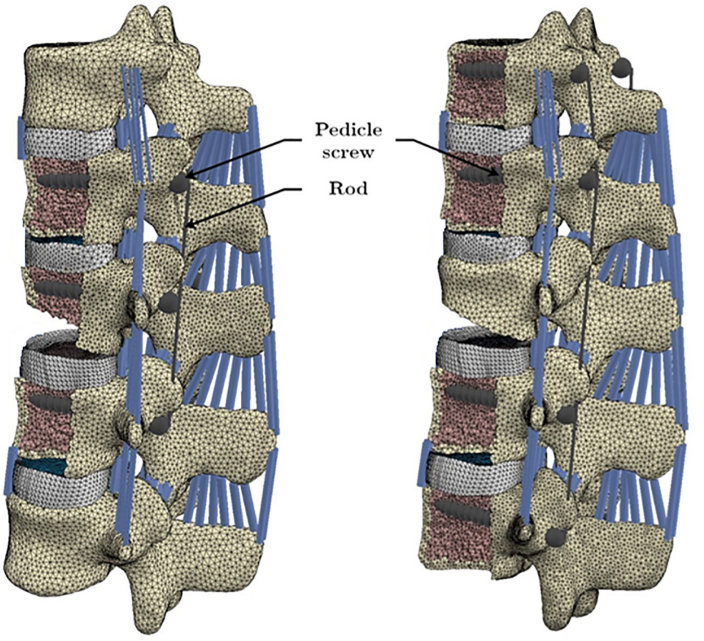

Figure 5.
FE models of the (a) PSS technique, including a view cut of T12, L1 and L2 vertebrae to demonstrate the screw insertion and (b) PL technique, including a view cut of T11, T12, L2 and L3 to enable the visualization of the screws

Source(s): Authors' own creation

surfaces. Conversely, the interaction between adjacent facet joints was implemented using a surface-to-surface contact condition that allows relative displacements.

In the pathological models, the connections between the pedicle screw and the vertebral bone as well as between the pedicle screw and the rod, were considered tied.

2.5 Mechanical properties

The mechanical properties for the bone, cartilaginous endplates, ligaments, fixation rods and screws are shown in Table 1. The mentioned structures were modeled considering a linear mechanical behavior (Chen *et al.*, 2001; de Visser *et al.*, 2007; Dreischarf *et al.*, 2014; Hato *et al.*, 2007; Sylvestre *et al.*, 2007). For the rods and screws, the mechanical properties of a titanium alloy were used (Chosa *et al.*, 2004; Xiao *et al.*, 2012). This material presents good biological and mechanical compatibility with human bones (Andreoni and Yip, 2020).

The intervertebral disc was considered hyperelastic, with material parameters presented in Table 2. Since the nucleus pulposus behaves as an incompressible material, the isotropic Neo-Hookean model was considered. For the annulus fibrosus, the hyperelastic transversely isotropic Holzapfel–Gasser–Ogden constitutive model was considered (Moramarco *et al.*, 2010; O'Connell *et al.*, 2009).

2.6 Range of motion

As previously mentioned, a load of 5 Nm was applied for flexion, extension, lateral bending and axial rotation motions. For the different scenarios, the results were measured at different dorsolumbar spine levels using the range of motion (ROM), expressed in degrees.

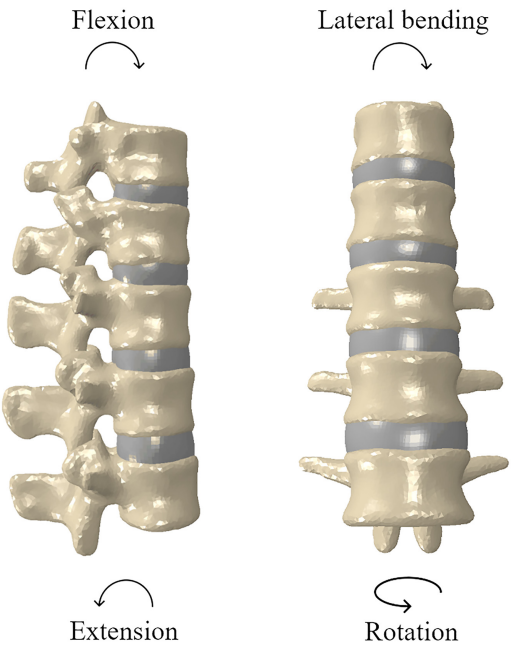

Source(s): Authors' own creation

Figure 6. Representation of the mechanical loading conditions implemented: flexion, extension, lateral bending and axial rotation

Component	C_{10} [MPa]	D [MPa^{-1}]	k_1 [MPa]	k_2 [−]	k
Nucleus pulposus	0.16	0.024	–	–	–
Annulus fibrosus	0.035	0	0.296	65	0

Source(s): Authors' own creation

Table 2. Hyperelastic mechanical properties of the intervertebral disc

First, a vector was calculated for each vertebra by selecting two nodes arbitrarily on the same vertebra. One node was positioned on the surface of the superior vertebral endplate, and the other on the surface of the inferior endplate. Second, the angle between the vectors of two adjacent vertebrae (T11–T12, T12–L1, L1–L2, and L2–L3 FSU) was calculated, as illustrated in Figure 7.

Since each movement can be analyzed in a single plane, to facilitate the analysis, the vectors were defined within the specific plane of motion. Finally, the result in interest of each FSU angular displacement (ROM) was obtained by the difference between the calculated functional unit angle (θ_i) in the model with no load applied and the angle (θ_f) of the corresponding functional unit in its full motion, θ_i–θ_f.

3. Results

3.1 Validation

The ROM obtained for the control model was compared with the following experimental results: Yamamoto *et al.* (1989) with a 10 Nm load, Oxland *et al.* (1992) with a 7.5 Nm load, Couvertier *et al.* (2017) with a 5 Nm load and Busscher *et al.* (2011) with a 4 Nm (Figure 8).

All these studies have the T11 superior endplate as the point of application, except for Yamamoto *et al.* (1989), which applied the load in the L1 vertebra.

The ROM obtained in the present study is consistent with the results obtained by Couvertier *et al.* (2017) and Busscher *et al.* (2011) for all load cases. For flexion, Yamamoto *et al.* (1989) significantly surpass other studies, consistent with the application of the highest load. For the extension, the ROM obtained by Yamamoto *et al.* (1989) is notably greater. Similar findings are observed for the ROM obtained by Oxland *et al.* (1992) with a 7.5 Nm load, specifically for the T12–L1 FSU. Results for lateral bending and axial rotation motions fall within the range of the experimental values. Lastly, calculated ROM values exceed the

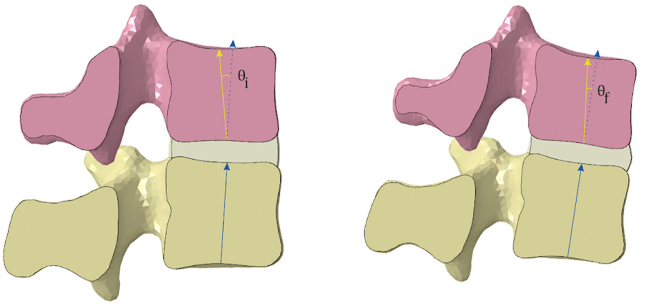

Figure 7.
Example of the angles between T11–T12 vertebrae for the initial (left) and final (right) positions

Source(s): Authors' own creation

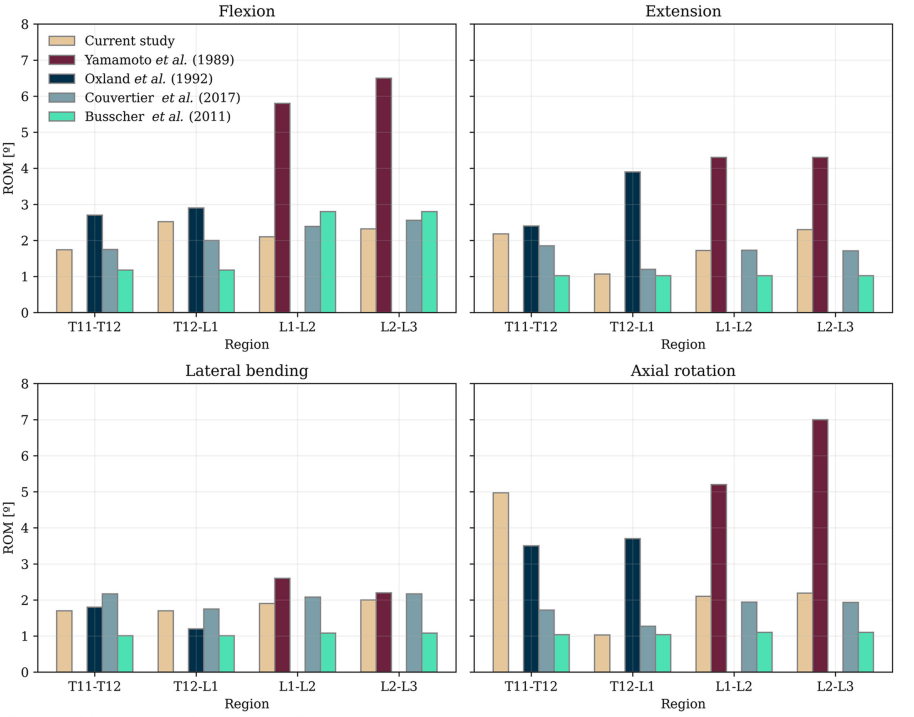

Figure 8.
ROM literature values: Yamamoto *et al.* (1989) with a 10 Nm load, Oxland *et al.* (1992) with a 7.5 Nm load, Couvertier *et al.* (2017) with a 5 Nm load and Busscher *et al.* (2011) with a 4 Nm load compared to a load of 5 Nm applied in the present study

Source(s): Authors' own creation

experimental ones for the T11–T12 region, while for the other regions, the obtained values correlate with the cadaveric ROM data.

3.2 Unstable complete burst model

Figure 9 presents the ROM values obtained for the complete burst model in comparison to the control model.

For the unstable complete burst model, the ROM values' sum is higher than the healthy ones in all case scenarios. In the burst model, the low resistance of the fractured L1 vertebra leads to significantly greater ROM values at T12–L1 and L1–L2 levels.

The flexion case presents the smallest ROM values, with both ends of the total model segment showing similarly limited ROM, measuring 1.73° in the T11–T12 and 1.89° in L2–L3 FSU. A comparable pattern is observed in the lateral bending load case, as the ligaments involved in this motion are preserved. The T11–T12 and L2–L3 FSU demonstrate nearly identical ROM values as in the previously mentioned case. However, extension ROM values are notably higher, particularly in the T12–L1 and L1–L2 FSU. The axial rotation load case yields the highest ROM values in the burst region. Since ALL ligaments were not considered, this load case results in the greatest rotations in the T12–L1 and L1–L2 FSU, measuring 50.01° and 33.67°, respectively.

3.3 PSS fixation with intermediate screws

Since the PSS procedure only fixates the T12–L1 and L1–L2 segments, ROM was only calculated in these two functional units (Table 3).

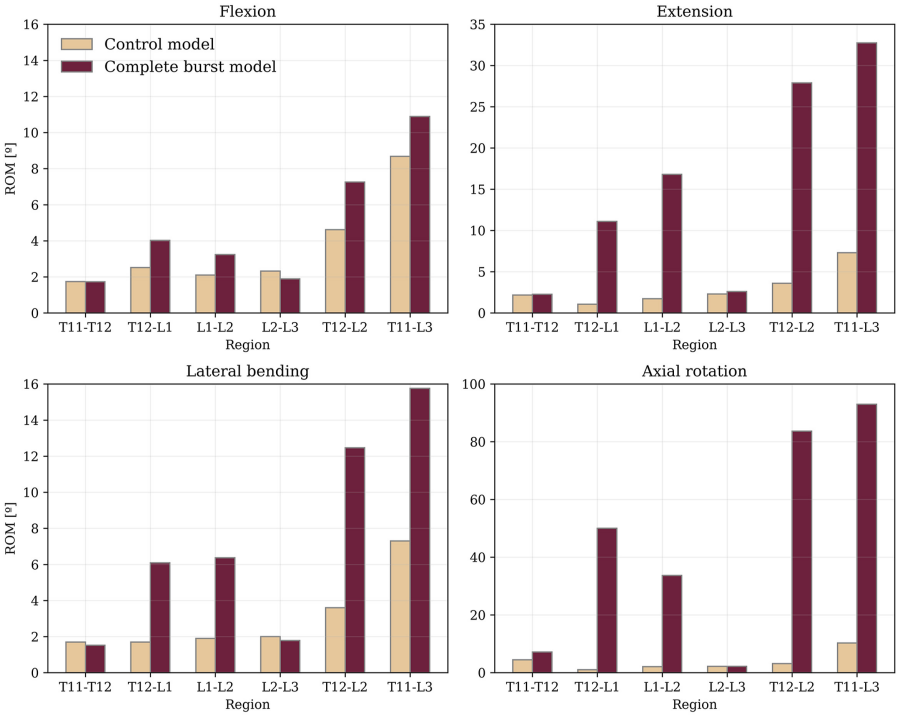

Source(s): Authors' own creation

Figure 9. Comparison of the ROM values between the control model and the complete burst model, including the sum of the obtained values between T12 and L2 vertebrae and between T11 and L2 vertebrae

As in the burst model, the flexion load case presents the lowest ROM values. The lateral bending motion presents a total ROM sum equal to 4.13°, greater than the previous one for the flexion load case. In this motion, the smallest ROM equal to 0.25° is found at the L1–L2 level, while the T12–L1 FSU ROM value is equal to 3.88°. The extension load case presents a total ROM sum equal to 4.40°, similar to the previous one for lateral bending. However, in this motion, the highest ROM value equal to 3.54° is found at the L1–L2 level, while the T12–L1 FSU ROM value is equal to 0.87°. The highest ROM values occur in axial rotation load, with 32.29° and 12.74° of ROM from up-down.

The screws from PSS are submitted to different mechanical efforts. The maximum principal stress values verified in the most loaded screws are included in Table 4. For each range of motion, the maximum stress value in the screw and the respective location are indicated.

Axial rotation leads to considerably larger stresses in the screws than in the other range of motions. Besides, lateral bending also creates larger stresses than extension and flexion. The location of the most loaded screws varies for different ranges of motions.

3.4 PL fixation

The PL fixation involves the fixation of all four FSU, from T11 to L3. Although the L1 vertebra lacks pedicle screws, its movement is restricted by the adjacent fixated vertebrae.

Table 5 illustrates the ROM values obtained for the PL fixation technique. Similar to the burst model, the T12–L1 and L1–L2 levels display greater ROM than the other levels. It can be observed that, for the PL model, the highest ROM values occur during axial rotation load, specifically at T12–L1 and L1–L2 levels, with 23.25° and 25.29°, respectively. For the other load cases, ROM values are comparable and all less than or equal to 1°, even at T12–L1 and L1–L2 levels.

Table 3.
PSS fixation model ROM [°] values

Region	Flexion	Extension	Lateral bending	Axial rotation
T12–L1	0.72	0.87	3.88	32.29
L1–L2	1.96	3.54	0.25	12.74

Source(s): Authors' own creation

Table 4.
Maximum principal stress values verified in the most loaded screws from PSS and respective locations

	Flexion	Extension	Lateral bending	Axial rotation
Stress [MPa]	34.39	49.60	83.69	202.8
Location	L2	T12	T12	L1

Source(s): Authors' own creation

Table 5.
PL fixation model ROM [°] values

Region	Flexion	Extension	Lateral bending	Axial rotation
T11–T12	0.15	0.13	0.05	3.62
T12–L1	1.00	0.56	0.01	23.25
L1–L2	0.79	0.90	0.37	25.29
L2–L3	0.32	0.12	0.10	0.25

Source(s): Authors' own creation

The screws from PL also withstand different loads. Similarly to PSS, the maximum principal stress values verified in the most loaded screws are included in Table 6.

Axial rotation also leads to considerably larger stresses in the screws than in the other range of motions. Besides, the location of the most loaded screws is constant for almost every range of motion (T11), except for axial rotation (T12).

Figure 10 presents vertebra displacements for all considered load cases of both PSS and PL techniques.

Figure 11 illustrates a comparison of the ROM values for the control model, complete burst model and the models with the two fixation techniques under study.

4. Discussion and conclusions

The present study introduces a computational model to simulate a dorsolumbar complete burst fracture. The primary objective is to conduct a biomechanical analysis, comparing the efficacy of two distinct fixation methods in addressing this specific type of fracture. This study seeks to advance our understanding of the mechanical implications associated with the chosen fixation approaches, contributing valuable insights to the field of orthopedic research.

Table 6. Maximum principal stress values verified in the most loaded screws from PL and respective locations

	Flexion	Extension	Lateral bending	Axial rotation
Stress [MPa]	28.65	28.65	49.03	197.2
Location	T11	T11	T11	T12

Source(s): Authors' own creation

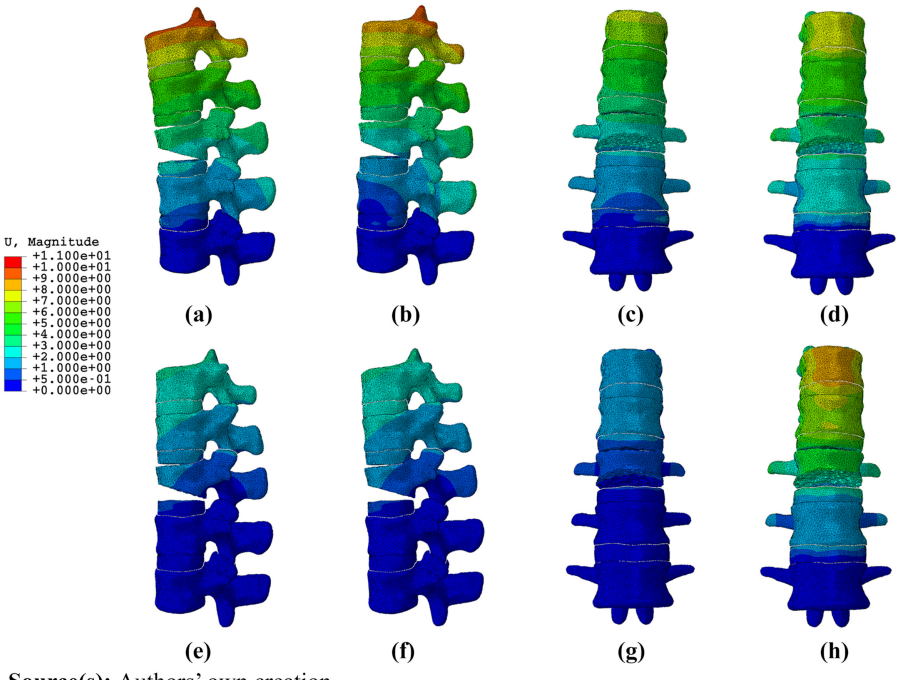

Source(s): Authors' own creation

Figure 10. PL fixation displacements (mm) for the different motions: (a) PSS flexion, (b) PSS extension, (c) PSS lateral bending, (d) PSS axial rotation, (e) PL flexion, (f) PL extension, (g) PL lateral bending and (h) PL axial rotation

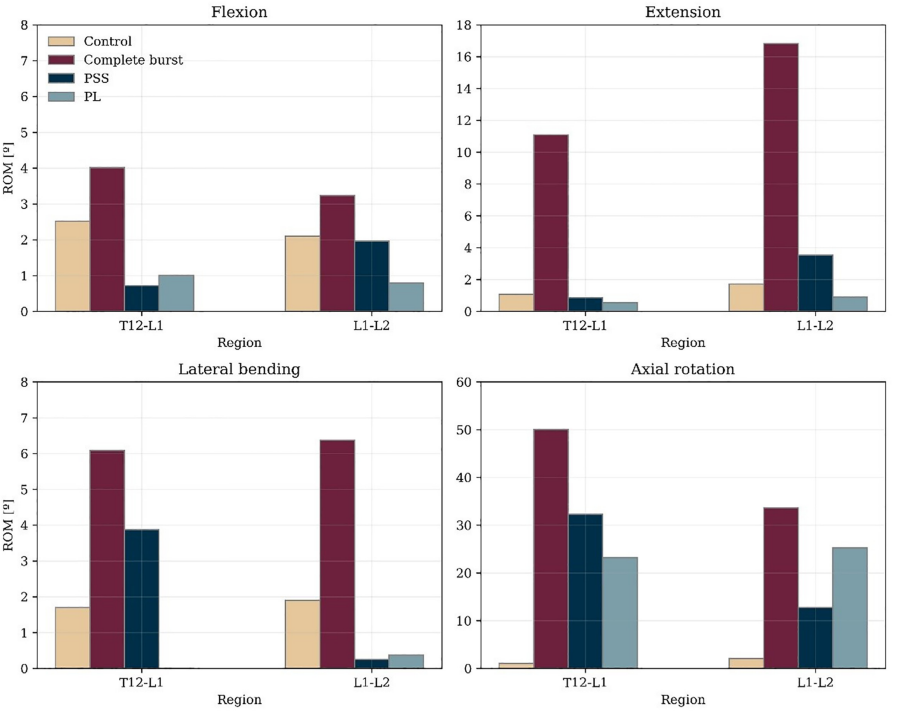

Figure 11.
Comparison of the ROM values between the control model, complete burst model, PSS fixation and PL fixation for the T12–L1 and L1–L2 levels

Source(s): Authors' own creation

Both PSS and PL fixation methods yield similar maintenance of sagittal alignment, kyphosis correction, neurological pain reduction and biomechanical behavior factors in terms of clinical results (Tian *et al.*, 2011; Vaccaro *et al.*, 1995; Jay and Ahn, 2013). However, it is not possible to distinguish between the two approaches based on their displacement in a clinical setting.

When comparing the complete burst model to the control model (considered healthy), there are no major differences observed in the flexion case. However, notable distinctions arise in the other three cases, where ROM values are significantly higher in the complete burst model, particularly at the T12–L1 and L1–L2 levels. This can be attributed to the weaker ALL ligaments and the more substantial weakening of the anterior region of the vertebra, a consequence of the L1 burst fracture.

To comprehend the impact of each fixation technique, it is imperative to compare it with the fractured model. In the case of PSS fixation with intermediate screws, the ROM values in the axial rotation load scenario are significantly increased. As rods have resistance to bending but lack resistance to axial rotation, they permit slight torsional freedom. Nevertheless, when compared with the burst model, the PSS fixation results in a lower rotation angle, attributed to vertebral fixation. In the other scenarios, values demonstrate a marked reduction with fixation, as expected.

With the PL technique, the ROM values were lower in comparison to the PSS, except for axial rotation at the L1–L2 level. This discrepancy can be attributed to the absence of a screw fixation for the L1 vertebra in the PL fixation, which allows a greater rotation in the fractured area than the other technique. Consequently, axial rotation at this level is allowed, resulting in values higher than those obtained with the PSS technique. Nevertheless, the rotational movement is still lower than in the case of the complete burst model.

Overall, the results reveal significant differences in the kinematic response of the dorsolumbar FSU depending on the intervertebral level and the load case. This study demonstrates that both models effectively stabilize the segment of interest. The PL fixation exhibits less movement freedom, becoming more stable than the PSS fixation. Thus, the PL technique is the optimal choice for an unstable fracture, as it results in a stiffer spine segment. Conversely, if the surgeon's objective is to minimize spine movements and the fracture is relatively stable, the PSS approach could be considered.

A recent study from Limthongkul *et al.* (2023) also analyzed various fixation techniques in a case of burst fracture of L1. The authors applied a compressive load to the superior surface of the T11 vertebra and analyzed displacement and stresses. The results obtained demonstrate that PL fixation allows for lower movement freedom, consistent with the findings of the present study.

The results presented are in accordance with the literature, since generally the long segment fixation technique allows a lower ROM (Basaran *et al.*, 2019; Wang *et al.*, 2019).

The limitations of the present study include the omission of soft tissues, spinal musculature and the rib cage as well as the simplified mechanical characterization of the bone, which was conducted using homogeneous material instead of a heterogeneous material mapped based on CT scans. These limitations highlight the necessity for additional research and refinement of computational models. A comprehensive understanding of dorsolumbar spine ROM is crucial for the development and evaluation of devices intended for intervertebral fixation. Future studies could address these limitations, incorporating a more detailed anatomical representation to enhance the clinical relevance of computational simulations in informing surgical decision-making and device design.

In conclusion, the computational study provides valuable insights into the biomechanical implications of different fixation methods for dorsolumbar complete burst fractures. The results affirm the suitability of finite element simulations for such investigations, enabling a detailed analysis of the spine's kinematic response without the ethical and practical challenges associated with other research methodologies.

References

Andreoni, W. and Yip, S. (2020), *Handbook of Materials Modeling: Applications: Current and Emerging Materials*, Springer International Publishing, New York City.

Areias, B., Caetano, S.C., Sousa, L.C., Parente, M., Jorge, R.N., Sousa, H. and Gonçalves, J.M. (2020), "Numerical simulation of lateral and transforaminal lumbar interbody fusion, two minimally invasive surgical approaches", *Computer Methods in Biomechanics and Biomedical Engineering*, Vol. 23 No. 8, pp. 408-421, doi: 10.1080/10255842.2020.1734579.

Basaran, R., Efendioglu, M., Kaksi, M., Celik, T., Mutlu, İ. and Ucar, M. (2019), "Finite element analysis of short- versus long-segment posterior fixation for thoracolumbar burst fracture", *World Neurosurgery*, Vol. 128, pp. e1109-e1117, doi: 10.1016/j.wneu.2019.05.077.

Bianco, R.-J., Arnoux, P.-J., Mac-Thiong, J.-M. and Aubin, C.-E. (2019), "Thoracic pedicle screw fixation under axial and perpendicular loadings: a comprehensive numerical analysis", *Clinical Biomechanics*, Vol. 68, pp. 190-196, doi: 10.1016/j.clinbiomech.2019.06.010.

Busscher, I., van Dieën, J.H., van der Veen, A.J., Kingma, I., Meijer, G.J.M., Verkerke, G.J. and Veldhuizen, A.G. (2011), "The effects of creep and recovery on the in vitro biomechanical characteristics of human multi-level thoracolumbar spinal segments", *Clinical Biomechanics*, Vol. 26 No. 5, pp. 438-444, doi: 10.1016/j.clinbiomech.2010.12.012.

Chen, C.-S., Cheng, C.-K., Liu, C.-L. and Lo, W.-H. (2001), "Stress analysis of the disc adjacent to interbody fusion in lumbar spine", *Medical Engineering & Physics*, Vol. 23 No. 7, pp. 485-493, doi: 10.1016/S1350-4533(01)00076-5.

Cheung, J. T.-M., Zhang, M. and Chow, D. H.-K. (2003), "Biomechanical responses of the intervertebral joints to static and vibrational loading: a finite element study", *Clinical Biomechanics*, Vol. 18 No. 9, pp. 790-799, doi: 10.1016/S0268-0033(03)00142-6.

Chosa, E., Goto, K., Totoribe, K. and Tajima, N. (2004), "Analysis of the effect of lumbar spine fusion on the superior adjacent intervertebral disk in the presence of disk degeneration, using the three-dimensional finite element method", *Journal of Spinal Disorders*, Vol. 17 No. 2, pp. 134-139, doi: 10.1097/00024720-200404000-00010.

Couvertier, M., Germaneau, A., Saget, M., Dupré, J.-C., Doumalin, P., Brémand, F., Hesser, F., Brèque, C., Roulaud, M., Monlezun, O., Vendeuvre, T. and Rigoard, P. (2017), "Biomechanical analysis of the thoracolumbar spine under physiological loadings: experimental motion data corridors for validation of finite element models", *Proceedings of the Institution of Mechanical Engineers, Part H: Journal of Engineering in Medicine*, Vol. 231 No. 10, pp. 975-981, doi: 10.1177/0954411917719740.

de Visser, H., Adam, C.J., Crozier, S. and Pearcy, M.J. (2007), "The role of quadratus lumborum asymmetry in the occurrence of lesions in the lumbar vertebrae of cricket fast bowlers", *Medical Engineering & Physics*, Vol. 29 No. 8, pp. 877-885, doi: 10.1016/j.medengphy.2006.09.010.

Dreischarf, M., Zander, T., Shirazi-Adl, A., Puttlitz, C.M., Adam, C.J., Chen, C.S., Goel, V.K., Kiapour, A., Kim, Y.H., Labus, K.M., Little, J.P., Park, W.M., Wang, Y.H., Wilke, H.J., Rohlmann, A. and Schmidt, H. (2014), "Comparison of eight published static finite element models of the intact lumbar spine: predictive power of models improves when combined together", *Journal of Biomechanics*, Vol. 47 No. 8, pp. 1757-1766, doi: 10.1016/j.jbiomech.2014.04.002.

Fennell, V.S., Palejwala, S., Skoch, J., Stidd, D.A. and Baaj, A.A. (2014), "Freehand thoracic pedicle screw technique using a uniform entry point and sagittal trajectory for all levels: preliminary clinical experience: clinical article", *Journal of Neurosurgery: Spine*, Vol. 21 No. 5, pp. 778-784, doi: 10.3171/2014.7.SPINE1489.

Fidalgo, D.S., Areias, B., Sousa, L.C., Parente, M., Jorge, R.N., Sousa, H. and Gonçalves, J.M. (2020), "Minimally invasive transforaminal and anterior lumbar interbody fusion surgery at level L5-S1", *Computer Methods in Biomechanics and Biomedical Engineering*, Vol. 23 No. 8, pp. 384-395, doi: 10.1080/10255842.2020.1731482.

Frost, B., Camarero-Espinosa, S. and Foster, E. (2019), "Materials for the spine: anatomy, problems, and solutions", *Materials*, Vol. 12 No. 2, p. 253, doi: 10.3390/ma12020253.

Fujimoto, T., Sei, A., Taniwaki, T., Okada, T., Yakushiji, T. and Mizuta, H. (2012), "Pedicle screw diameter selection for safe insertion in the thoracic spine", *European Journal of Orthopaedic Surgery & Traumatology*, Vol. 22 No. 5, pp. 351-356, doi: 10.1007/s00590-011-0846-2.

Hato, T., Kawahara, N., Tomita, K., Murakami, H., Akamaru, T., Tawara, D., Sakamoto, J., Oda, J. and Tanaka, S. (2007), "Finite-element analysis on closing-opening correction osteotomy for angular kyphosis of osteoporotic vertebral fractures", *Journal of Orthopaedic Science*, Vol. 12 No. 4, pp. 354-360, doi: 10.1007/s00776-007-1144-z.

Hershkovitz, Y., Sheffer, D., Peleg, K., Kessel, B., Dubose, J.J., Jeroukhimov, I., Givon, A., Dudkiewicz, M. and Aranovich, D. (2021), "Thoracic vertebrae fracture: is it an indicator of abdominal injury?", *The American Journal of Emergency Medicine*, Vol. 43, pp. 235-237, doi: 10.1016/j.ajem.2020.03.016.

Jay, B. and Ahn, S. (2013), "Vertebroplasty", *Seminars in Interventional Radiology*, Vol. 30 No. 03, pp. 297-306, doi: 10.1055/s-0033-1353483.

Lehman, R.A., Polly, D.W., Kuklo, T.R., Cunningham, B., Kirk, K.L. and Belmont, P.J. (2003), "Straight-forward versus anatomic trajectory technique of thoracic pedicle screw fixation: a biomechanical analysis", *Spine*, Vol. 28 No. 18, pp. 2058-2065, doi: 10.1097/01.BRS.0000087743.57439.4F.

Lenke, L. and Kim, Y. (2005), "Thoracic pedicle screw placement: free-hand technique", *Neurology India*, Vol. 53 No. 4, p. 512, doi: 10.4103/0028-3886.22622.

Liang, C., Liu, G., Liang, G., Zheng, X., Yin, D., Xiao, D., Zeng, S., Cai, H. and Chang, Y. (2020), "Healing pattern classification for thoracolumbar burst fractures after posterior short-segment fixation", *BMC Musculoskeletal Disorders*, Vol. 21 No. 1, p. 373, doi: 10.1186/s12891-020-03386-z.

Limthongkul, W., Wannaratsiri, N., Sukjamsri, C., Benyajati, C., Limthongkul, P., Tanasansomboon, T., Yingsakmongkol, W. and Singhatanadgige, W. (2023), "Biomechanical comparison between posterior long-segment fixation, short-segment fixation, and short-segment fixation with intermediate screws for the treatment of thoracolumbar burst fracture: a finite element analysis", *International Journal of Spine Surgery*, Vol. 17 No. 3, pp. 442-448, doi: 10.14444/8441.

Mahadevan, V. (2018), "Anatomy of the vertebral column", *Surgery (Oxford)*, Vol. 36 No. 7, pp. 327-332, doi: 10.1016/j.mpsur.2018.05.006.

Marchand, F. and Ahmed, A.M. (1990), "Investigation of the laminate structure of lumbar disc anulus fibrosus", *Spine*, Vol. 15 No. 5, pp. 402-410, doi: 10.1097/00007632-199005000-00011.

Minamide, A., Maeda, T., Yamada, H., Murakami, K., Okada, M., Enyo, Y., Nakagawa, Y., Iwasaki, H., Tsutsui, S., Takami, M., Nagata, K., Hashizume, H., Yukawa, Y., Schoenfeld, A.J. and Simpson, A.K. (2018), "Early versus delayed kyphoplasty for thoracolumbar osteoporotic vertebral fractures: the effect of timing on clinical and radiographic outcomes and subsequent compression fractures", *Clinical Neurology and Neurosurgery*, Vol. 173, pp. 176-181, doi: 10.1016/j.clineuro.2018.07.019.

Moon, S.M., Yoder, J.H., Wright, A.C., Smith, L.J., Vresilovic, E.J. and Elliott, D.M. (2013), "Evaluation of intervertebral disc cartilaginous endplate structure using magnetic resonance imaging", *European Spine Journal*, Vol. 22 No. 8, pp. 1820-1828, doi: 10.1007/s00586-013-2798-1.

Moramarco, V., Pérez del Palomar, A., Pappalettere, C. and Doblaré, M. (2010), "An accurate validation of a computational model of a human lumbosacral segment", *Journal of Biomechanics*, Vol. 43 No. 2, pp. 334-342, doi: 10.1016/j.jbiomech.2009.07.042.

Oxland, T.R., Lin, R. and Panjabi, M.M. (1992), "Three-Dimensional mechanical properties of the thoracolumbar junction", *Journal of Orthopaedic Research*, Vol. 10 No. 4, pp. 573-580, doi: 10.1002/jor.1100100412.

O'Connell, G.D., Guerin, H.L. and Elliott, D.M. (2009), "Theoretical and uniaxial experimental evaluation of human annulus fibrosus degeneration", *Journal of Biomechanical Engineering*, Vol. 131 No. 11, 111007, doi: 10.1115/1.3212104.

Sohn, S., Park, T.H., Chung, C.K., Kim, Y.J., Jang, J.W., Han, I. and Lee, S.J. (2018), "Biomechanical characterization of three iliac screw fixation techniques: a finite element study", *Journal of Clinical Neuroscience*, Vol. 52, pp. 109-114, doi: 10.1016/j.jocn.2018.03.002.

Soultanis, K., Thano, A. and Soucacos, P.N. (2021), "Outcome of thoracolumbar compression fractures following non-operative treatment", *Injury*, Vol. 52 No. 12, pp. 3685-3690, doi: 10.1016/j.injury.2021.05.019.

Svedmark, P., Tullberg, T., Noz, M.E., Maguire, G.Q., Zeleznik, M.P., Weidenhielm, L., Nemeth, G. and Olivecrona, H. (2012), "Three-dimensional movements of the lumbar spine facet joints and segmental movements: in vivo examinations of normal subjects with a new non-invasive method", *European Spine Journal*, Vol. 21 No. 4, pp. 599-605, doi: 10.1007/s00586-011-1988-y.

Sylvestre, P.-L., Villemure, I. and Aubin, C.-É. (2007), "Finite element modeling of the growth plate in a detailed spine model", *Medical & Biological Engineering & Computing*, Vol. 45 No. 10, pp. 977-988, doi: 10.1007/s11517-007-0220-z.

Tian, J.W., Wang, L., Xia, T., Liu, C.Y., Zhao, Q.H. and Dong, S.H. (2011), "Posterior short-segmental fixation combined with intermediate screws vs conventional intersegmental fixation for monosegmental thoracolumbar fractures", *Orthopedics*, Vol. 34 No. 8, pp. 389-396, doi: 10.3928/01477447-20110627-08.

Vaccaro, A., Rizzolo, S., Balderston, R., Allardyce, T.J., Garfin, S., Dolinskas, C. and An, H. (1995), "Placement of pedicle screws in the thoracic spine. Part I: morphometric analysis of the thoracic vertebrae", *The Journal of Bone and Joint Surgery. American Volume*, Vol. 77 No. 8, pp. 1193-1199, doi: 10.2106/00004623-199508000-00008.

Vos, T., Abajobir, A.A., Abate, K.H., Abbafati, C., Abbas, K.M., Abd-Allah, F., Abdulkader, R.S., Abdulle, A.M., Abebo, T.A., Abera, S.F., Aboyans, V., Abu-Raddad, L.J., Ackerman, I.N., Adamu, A.A., Adetokunboh, O., Afarideh, M., Afshin, A., Agarwal, S.K., Aggarwal, R. ... Murray, C.J.L. (2017), "Global, regional, and national incidence, prevalence, and years lived with disability for 328 diseases and injuries for 195 countries, 1990-2016: a systematic analysis for the Global Burden of Disease Study 2016", *The Lancet*, Vol. 390, No. 10100, pp. 1211-1259, doi: 10.1016/S0140-6736(17)32154-2.

Vu, C. and Gendelberg, D. (2020), "Classifications in brief: AO thoracolumbar classification system", *Clinical Orthopaedics & Related Research*, Vol. 478 No. 2, pp. 434-440, doi: 10.1097/CORR.0000000000001086.

Wade, K. (2018), "Vertebral endplates", in *Biomechanics of the Spine*, Elsevier, pp. 125-140, doi: 10.1016/B978-0-12-812851-0.00008-2.

Wang, W., Pei, B., Pei, Y., Shi, Z., Kong, C., Wu, X., Wu, N., Fan, Y. and Lu, S. (2019), "Biomechanical effects of posterior pedicle fixation techniques on the adjacent segment for the treatment of thoracolumbar burst fractures: a biomechanical analysis", *Computer Methods in Biomechanics and Biomedical Engineering*, Vol. 22 No. 13, pp. 1083-1092, doi: 10.1080/10255842.2019.1631286.

Xiao, Z., Wang, L., Gong, H. and Zhu, D. (2012), "Biomechanical evaluation of three surgical scenarios of posterior lumbar interbody fusion by finite element analysis", *BioMedical Engineering OnLine*, Vol. 11 No. 1, p. 31, doi: 10.1186/1475-925X-11-31.

Yamamoto, I., Panjabi, M.M., Crisco, T. and Oxland, T. (1989), "Three-dimensional movements of the whole lumbar spine and lumbosacral joint", *Spine*, Vol. 14 No. 11, pp. 1256-1260, doi: 10.1097/00007632-198911000-00020.

Zander, T., Dreischarf, M., Timm, A.-K., Baumann, W.W. and Schmidt, H. (2017), "Impact of material and morphological parameters on the mechanical response of the lumbar spine – a finite element sensitivity study", *Journal of Biomechanics*, Vol. 53, pp. 185-190, doi: 10.1016/j.jbiomech.2016.12.014.

Zhang, H. and Zhu, W. (2019), "The path to deliver the most realistic follower load for a lumbar spine in standing posture: a finite element study", *Journal of Biomechanical Engineering*, Vol. 141 No. 3, 031010, doi: 10.1115/1.4042438.

Zhifeng, S., Kaixiang, Y., Hongtao, C., Tao, S., Lei, Y., Dawei, G., Jian, T. and Xiaojian, C. (2018), "A novel entry point for pedicle screw placement in the thoracic spine", *The Journal of Biomedical Research*, Vol. 32 No. 2, p. 123, doi: 10.7555/JBR.31.20160037.

Corresponding author
Rita Moura can be contacted at: up201404216@edu.fe.up.pt